http://cpb.iphy.ac.cn
http://iopscience.iop.org/cpb
中国物理 B
Chinese Physics B

Self-assembled monolayer modified copper(I) iodide hole transport layer for efficient polymer solar cells

Yuancong Zhong(钟远聪), Qilun Zhang(张琪伦), You Wei(魏优), Qi Li(李琦), Yong Zhang(章勇)

Citation: Chin. Phys. B . 2018, 27(7): 078802. **doi:** 10.1088/1674-1056/27/7/078802

Journal homepage: http://cpb.iphy.ac.cn; http://iopscience.iop.org/cpb

What follows is a list of articles you may be interested in

Sodium chloride methanol solution spin-coating process for bulk-heterojunction polymer solar cells

Tong-Fang Liu(刘统方), Yu-Feng Hu(胡煜峰), Zhen-Bo Deng(邓振波), Xiong Li(李熊), Li-Jie Zhu(朱丽杰), Yue Wang(王越), Long-Feng Lv(吕龙锋), Tie-Ning Wang(王铁宁), Zhi-Dong Lou(娄志东), Yan-Bing Hou(侯延冰), Feng Teng(滕枫)
Chin. Phys. B . 2016, 25(8): 088801. **doi:** 10.1088/1674-1056/25/8/088801

Effects of acetone-soaking treatment on the performance of polymer solar cells based on P3HT/PCBM bulk heterojunction

Liu Yu-Xuan, Lü Long-Feng, Ning Yu, Lu Yun-Zhang, Lu Qi-Peng, Zhang Chun-Mei, Fang Yi, Tang Ai-Wei, Hu Yu-Feng, Lou Zhi-Dong, Teng Feng, Hou Yan-Bing
Chin. Phys. B . 2014, 23(11): 118802. **doi:** 10.1088/1674-1056/23/11/118802

Improved performance of P3HT：PCBM solar cells by both anode modification and short-wavelength energy utilization using $Tb(aca)_3phen$

Zhuo Zu-Liang, Wang Yong-Sheng, He Da-Wei, Fu Ming
Chin. Phys. B . 2014, 23(9): 098802. **doi:** 10.1088/1674-1056/23/9/098802

MoO_3/Ag/Al/ZnO intermediate layer for inverted tandem polymer solar cells

Qing Jian, Zhong Zhen-Feng, Liu Yong, Li Bao-Jun, Zhou Xiang
Chin. Phys. B . 2014, 23(3): 038802. **doi:** 10.1088/1674-1056/23/3/038802

Effects of annealing rate and morphology of sol–gel derived ZnO on the performance of inverted polymer solar cells

Yu Xuan, Hu Zi-Yang, Huang Zhen-Hua, Yu Xiao-Ming, Zhang Jian-Jun, Zhao Geng-Shen, Zhao Ying
Chin. Phys. B . 2013, 22(11): 118801. **doi:** 10.1088/1674-1056/22/11/118801

Self-assembled monolayer modified copper(I) iodide hole transport layer for efficient polymer solar cells*

Yuancong Zhong(钟远聪)[1,2], Qilun Zhang(张琪伦)[1], You Wei(魏优)[1], Qi Li(李琦)[1], and Yong Zhang(章勇)[1,†]

[1] *Guangdong Provincial Key Laboratory of Nanophotonic Functional Materials and Devices, Institute of Optoelectronic Material and Technology, South China Normal University, Guangzhou* 510631, *China*

[2] *School of Physics and Optical Information Technology, Jiaying University, Meizhou* 514015, *China*

(Received 7 March 2018; revised manuscript received 1 May 2018; published online 25 June 2018)

The morphology of the copper iodide (CuI) film as an inorganic p-type material has an important influence on enhancing the performance of polymer solar cells (PSCs). A self-assembled monolayer of 3-aminopropanoic acid (C_3-SAM) was used on the surface of indium tin oxide (ITO) before depositing the CuI films. Consequently, a well-distributed and smooth CuI film was formed with pinhole free and complete surface coverage. The root mean square of the corresponding CuI film was reduced from 3.63 nm for ITO/CuI to 0.77 nm. As a result, the average power conversion efficiency (PCE) of PSCs with the device structure of ITO/C_3-SAM/CuI/P3HT:PC_{61}BM/ZnO/Al increased significantly from 2.55% (best 2.66%) to 3.04% (best 3.20%) after C_3-SAM treatment. This work provides an effective strategy to control the morphology of CuI films through interfacial modification and promotes its application in efficient PSCs.

Keywords: polymer solar cell, copper(I) iodide, self-assembled monolayer, morphology

PACS: 88.40.jr, 72.80.Jc, 81.16.Dn, 68.55.–a **DOI:** 10.1088/1674-1056/27/7/078802

1. Introduction

Polymer solar cells (PSCs) have many unique advantages of easy manufacturing process, low-cost, light weight, mechanical flexibility, and so on. It is a very promising alternative in photovoltaic field.[1–5] In recent years, numerous strategies have been utilized to enhance the performance of PSCs, including the synthesis of efficient photoactive materials,[6,7] the modification of film morphology,[8,9] and the reasonable selection of transport layers.[10–13] Consequently, the power conversion efficiency (PCE) of PSCs has been significantly improved, and it is worth noting that the values were up to over 12% for nonfullerene polymer solar cells that fabricated by ternary bulk-heterojunction[14] or the molecular regulation of acceptors,[15,16] which will further accelerate the commercial application of PSCs. The widely used structure of PSCs is a sandwich structure of a hole transport layer (HTL), photoactive layer, and electron transfer layer (ETL). The most frequently used material of HTLs is poly(3,4-ethylenedioxythiophene):poly(styrenesulfonate) (PEDOT:PSS) for conventional PSCs. Although PEDOT:PSS has a high work function (5.0 eV), high conductivity, and smooth film, its acidic and hygroscopic natures can corrode the indium tin oxide (ITO) anode and deteriorate the device performance. Furthermore, PEDOT:PSS is not very effective to block electrons.[17–19]

In order to solve the above problems of PEDOT:PSS, various inorganic materials have been reported as efficient HTLs in PSCs, such as nickel oxide (NiO_x),[20] vanadium oxide (V_2O_5),[21] copper oxide (CuO),[22] and copper(I) thiocyanate (CuSCN).[23] Recently, due to the characteristics of suitable energy level, high transparency and solution-processed, γ-phase copper(I) iodide (CuI) as HTLs has also been employed in PSCs.[24–30] CuI is a p-type semiconductor with zinc blende structure and has a wide band gap of 3.1 eV. Shao *et al.*[24] first used p-type CuI as HTLs for high-efficiency poly(3-hexylthiophene):[6,6]-phenyl C61-butyric acid methyl ester (P3HT:PC_{61}BM) bulk-heterojunction solar cells, but the PCE of 2.6% achieved by a solution-processed CuI interfacial layer is lower than 3.1% with the vacuum deposited CuI layer. Subsequently, Sun *et al.*[25] reported that the PSCs based on a CuI layer spin-coated with an appropriate speed reached a very high PCE of 4.15% by increasing the thickness of organic active layer. However, the CuI interfacial layer prepared by spin-coating CuI dispersion on the surface of ITO easily forms large aggregates of CuI particles and island-style polycrystalline films,[24,29,31] leading to large leakage current and unintentionally direct short for the CuI-based PSCs.

In this work, we adopted solution-processed CuI films as HTLs for PSCs (device structure shown in Fig. 1), and found that the morphology of CuI films could be modified by a self-assembled monolayer of 3-aminopropanoic acid (C_3-SAM) absorbed on the surface of ITO before depositing CuI

*Project supported by the National Natural Science Foundation of China (Grant Nos. 61377065 and 61574064), the Science and Technology Planning Project of Guangdong Province, China (Grant Nos. 2013CB040402009 and 2015B010132009), and the Science and Technology Project of Guangzhou City, China (Grant No. 2014J4100056).

†Corresponding author. E-mail: zycq@scnu.edu.cn

© 2018 Chinese Physical Society and IOP Publishing Ltd

films. Consequently, a well-distributed and smooth CuI film was formed with pinhole free and complete surface coverage. The short-circuit current (J_{sc}) and PCE of PSCs increased from 8.69 mA/cm^2 and 2.55% to 9.52 mA/cm^2 and 3.04%, respectively. This simple and effective strategy should further promote the potential application of CuI inorganic p-type material in high performance PSCs.

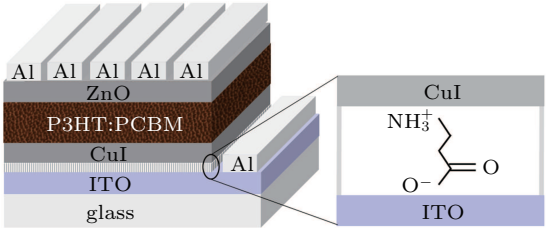


Fig. 1. (color online) Device structure of PSCs based on CuI as HTLs modified by C_3-SAM.

2. Experimental

2.1. Materials

PEDOT:PSS (AI 4083) was purchased from Heraeus. The 3-aminopropanoic, copper iodide (99.999%), anhydrous acetonitrile (99.8%), ZnO, and anhydrous 1,2-dichlorobenzene (99.8%) were purchased from Sigma-Aldrich. The poly(3-hexylthiophene) (P3HT) and [6,6]-phenyl C61-butyric acid methyl ester ($PC_{61}BM$) were purchased from Luminescence Technology Corp. These materials obtained from commercial way were used without further purification.

2.2. Device fabrication

The structure of the fabricated PSCs was ITO/HTLs/P3HT:$PC_{61}BM$/ZnO/Al (as shown in Fig. 1). The ITO coated glass substrates (15×15 mm^2) were dried at 90 °C for one night after a sequential ultrasonic treatment in deionized water, acetone, deionized water, and isopropanol for 10 min in each solution. To realize the effective deposition of C_3-SAM, some cleaned ITO substrates were dipped into 3-aminopropanoic acid solution dissolved in deionized water (1 mg/ml) at 70 °C for 2 h. After immersion, the ITO substrates were rinsed with deionized water to remove excess molecules and dried at 55 °C for 30 min. The CuI dispersion in acetonitrile (10 mg/ml) was spin-coated at 2000 rpm for 40 s on the cleaned ITO or C_3-SAM treated ITO substrates in a glove box. PEDOT:PSS was filtered with a 0.45 μm filter and spin-coated on the cleaned ITO substrates pre-treated by ultraviolet (UV)-ozone plasma at 3500 rpm for 40 s, and then PEDOT:PSS films (about 40 nm) were baked at 120 °C for 30 min on a hot plate in air. Next, the photoactive layer was spin-coated on the PEDOT:PSS or CuI layer from a solution with P3HT:$PC_{60}BM$ ratio of 1:0.8 (P3HT concentration of 20 mg/ml) in 1,2-dichlorobenzene/1,8-diiodooctane (50:1 vol%) mixed solvent at 800 rpm for 45 s and then annealed at 150 °C for 15 min after a placement of 7 h. The ZnO nanocrystals (in ethanol, 1 wt.%) were spin-coated on the P3HT:$PC_{61}BM$ layer and then annealed at 120 °C for 15 min to remove the residual solvent. Finally, the device fabrication was finished by thermal evaporation of 100 nm Al as the cathode under a vacuum less than 3×10^{-4} Pa. The active area of the fabricated device was 0.15 cm^2.

2.3. Characterization

The UV-visible absorbance spectra and the x-ray diffraction (XRD) patterns of CuI films were recorded by an ultraviolet-visible (UV-vis) spectrometer (Agilent Technologies 8453 A) and x-ray diffractometer (Bruker D8 Advance), respectively. The surface morphologies of CuI films were analyzed with the atomic force microscopy (AFM, NT-MDT) and scanning electron microscopy (SEM, ZEISS Ultra 55). The distribution of copper (Cu) and iodine (I) elements in the CuI films was investigated utilizing a distribution mapping technique of energy-dispersive x-ray spectroscope (EDS). The current density–voltage (J–V) characteristics of the devices were measured through a Keithley 2400 source measurement system under the illumination of 100 mW/cm^2 of AM1.5 G (Oriel model 91160) and in the dark. An optical contact angle meter (OCA20, Data physics) with tilting table was used to carry out contact angle measurements of ITO substrates under an ambient atmosphere. The external quantum efficiency (EQE) measurements were performed by solar cell spectral response measurement system QE-R3011 (Enlitechnology Co. Ltd, Taiwan, China).

3. Results and discussion

The water contact angle measurement was carried out to explore the surface characteristics of ITO treated by C_3-SAM. Figure 2(a) shows the contact angle change of the ITO surface after the treatment of C_3-SAM. It can be observed that the contact angle of ITO was reduced from 76.78° to 47.16° after C_3-SAM modifying. The contact angle change should be related to the C_3-SAM self-assembled on the surface of ITO because the 3-aminopropanoic acid molecule has the hydrophobic –COOH and –NH_2 groups, indicating that the C_3-SAM molecules had been absorbed on the surface of ITO.

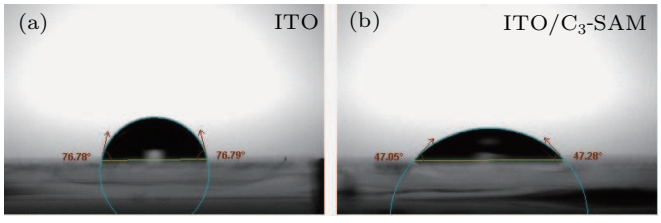


Fig. 2. (color online) Water contact angle images of (a) ITO and (b) ITO/C_3-SAM.

Figure 3(a) shows the XRD patterns of CuI films spin-coated on raw ITO and C_3-SAM treated ITO substrates. The positions of diffraction peaks of the two XRD patterns were the same. The peaks at 26° and 52.3° are attributed to the (111) and (222) faces of the γ-phase CuI with a zinc blende structure, respectively. The intensity of diffraction peak of CuI films is reduced after C_3-SAM treatment. According to the Scherrer equation[32,33]

$$D = \frac{k\lambda}{B\cos\theta},$$

where $k = 0.89$ is the constant of Scherrer, $\lambda = 0.154056$ nm is the wavelength of x-ray, B is the full width at half maximum (FWHM) of diffraction peak, and θ is the diffraction angle. The average crystallite size (D) of CuI nanoparticles is reduced from 26.31 nm to 24.88 nm after C_3-SAM modification. The smaller crystallite size of CuI nanoparticles with C_3-SAM is consistent with the reduced intensity of the corresponding diffraction peak. Figure 3(b) displays the UV-vis absorbance spectra of CuI films. The absorbance edge of CuI films with C_3-SAM modification has a bit blue shift relative to that without C_3-SAM, which further confirmed the decrease of crystallite size of CuI nanoparticles after C_3-SAM modification.

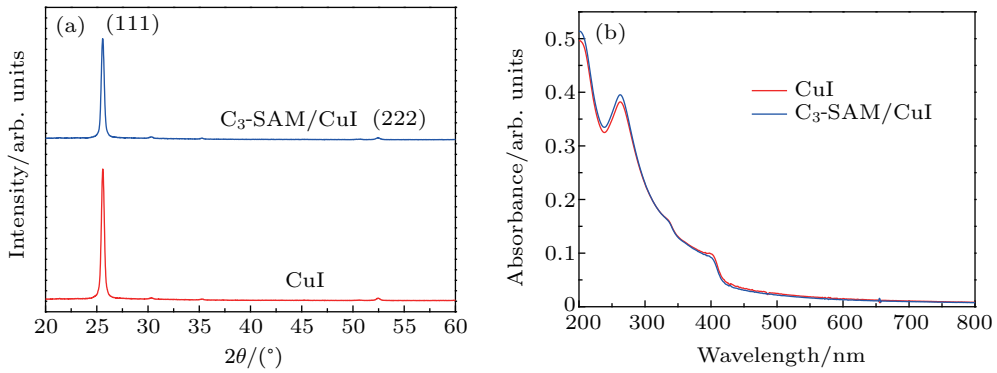


Fig. 3. (color online) (a) XRD patterns and (b) UV-visible absorbance spectra of CuI films with and without C_3-SAM modification.

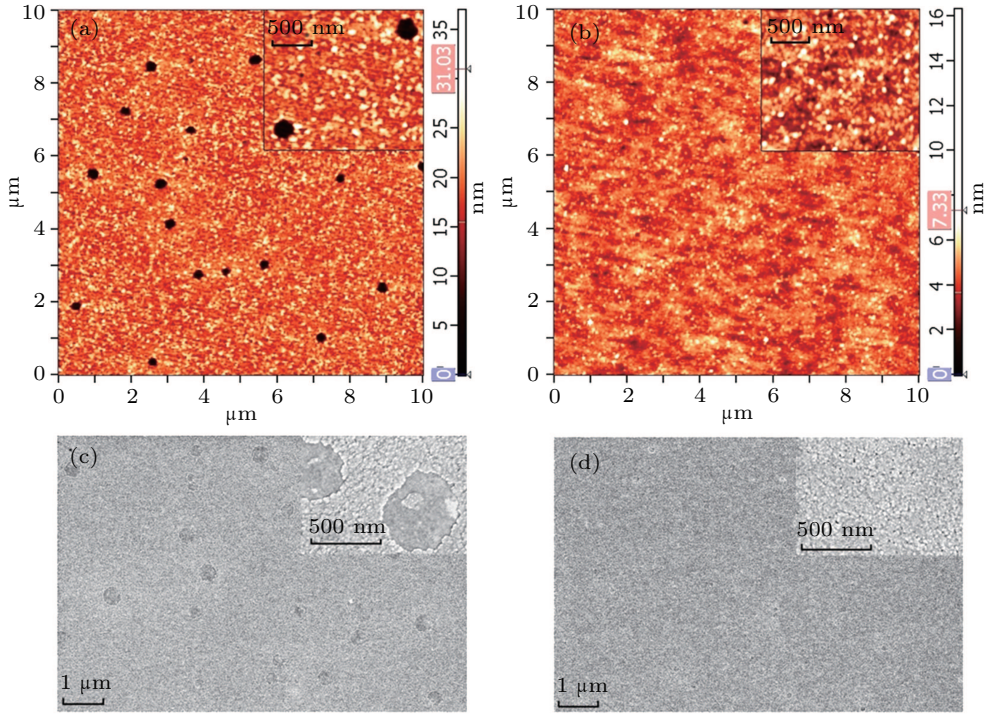


Fig. 4. (color online) AFM images of CuI films (a) without and (b) with C_3-SAM modification. SEM images of CuI films (c) without and (d) with C_3-SAM modification. Insets show partial images at high magnification.

To reveal the effect of C_3-SAM on the morphology of CuI films, the surface morphology of CuI films has been investigated by the atomic force microscopy (AFM) and scanning electron microscope (SEM). The AFM image of CuI film spin-coated on the surface of raw ITO is exhibited in Fig. 4(a), which shows a high density of pinholes, resulting in a quite rough surface with a root-mean-square (RMS) of 3.63 nm. In contrast, the CuI film after C_3-SAM treatment exhibits pin-

hole free and uniform CuI coverage in Fig. 4(b), and the RMS of the corresponding CuI film is only 0.77 nm. It can be observed from Figs. 4(c) and 4(d) that the SEM images of CuI films clearly illustrate the morphology changes after C_3-SAM modification. The CuI films without C_3-SAM modification show many large hollows with the biggest diameters of about 650 nm. However, after C_3-SAM modification, the CuI film presents smooth and uniform surface morphology with a compact structure. The surface of ITO showed higher hydrophilicity after C_3-SAM treatment due to the reduced contact angle, which enhanced the wetting of CuI dispersion on the surface of ITO. As a result, the C_3-SAM on ITO can induce significant improvement of morphology of CuI films. In addition, the electrostatic interaction between the CuI and the amino group of 3-aminopropanoic acid can decrease the aggregations during the forming process of CuI films. The working mechanism for such changing morphology is similar to that reported by Zuo *et al.*[34] and Gu *et al.*[35]

Figure 5 displays the distribution mapping images of Cu and I elements from CuI films. It can be noted that the Cu and I distributions of CuI films with C_3-SAM modification are more uniform and dense than those without C_3-SAM, which further confirms that more CuI particles are absorbed on the surface of ITO by C_3-SAM treatment.

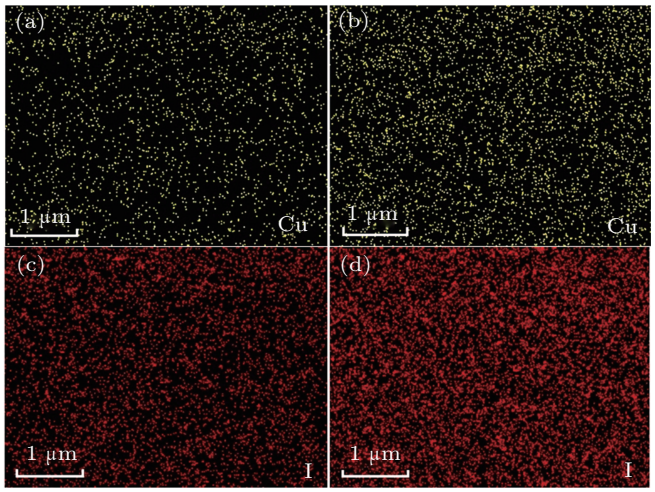


Fig. 5. (color online) The distribution mapping images of Cu element from CuI films (a) without and (b) with C_3-SAM modification, and I element from CuI films (c) without and (d) with C_3-SAM modification.

This pinhole free and uniform CuI film should be important to be used as HTLs of highly efficient PSCs. We fabricated the PSCs using PEDOT:PSS, CuI, and C_3-SAM/CuI as HTLs. The device structure is shown in Fig. 1. The corresponding *J*–*V* characteristics and the device parameters are shown in Fig. 6 and Table 1, respectively. The short-circuit current (J_{sc}) and PCE of PSCs increase from 8.69 mA/cm^2 and 2.55% for ITO/CuI HTL to 9.52 mA/cm^2 and 3.04% for ITO/C_3-SAM/CuI HTL, respectively. Figure 6(b) displays that the dark current density of the C_3-SAM/CuI devices is lower than that of the CuI devices, which indicates this uniform and pinhole free CuI can reduce the leakage current and block electrons. In addition, after C_3-SAM modification, the open-circuit voltage (V_{oc}) and fill factor (FF) values also increase from 0.54 V and 54.15% to 0.55 V and 56.43%, respectively. Combining all of these improved factors, the PSCs based on ITO/C_3-SAM/CuI achieved the highest PCE of 3.20% comparing with 3.18% of PSCs using PEDOT:PSS as HTL. The improved performance of PSCs should be attributed to the C_3-SAM that induced the morphology improvement of CuI films during the solution-processing. Although the V_{oc} of the PSC based on C_3-SAM/CuI as HTL was lower than that of the PEDOT:PSS-based PSC, the other device performance was almost the same as that of the PEDOT:PSS-based devices. Figure 7 plots the EQE of the corresponding PSCs. It can be found that the EQE of PSCs based on C_3-SAM/CuI as HTLs is higher than that of PSCs without C_3-SAM treatment. The improved EQE spectrum with C_3-SAM treatment agrees well with the increased J_{sc}.

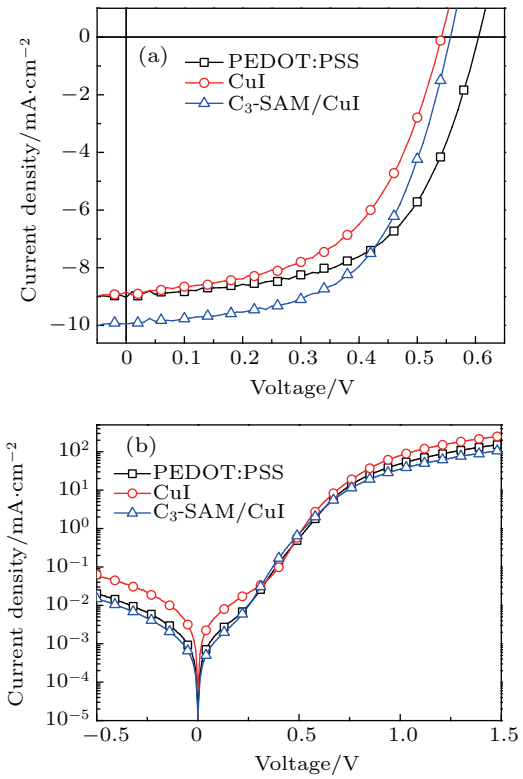


Fig. 6. (color online) *J*–*V* characteristics of PSCs with PEDOT:PSS, CuI, and C_3-SAM/CuI (a) under the illumination of AM1.5G, 100 mW/cm^2 and (b) under the dark condition.

Table 1. Summarized photovoltaic parameters of PSCs based on different HTLs.

HTLs	V_{oc}/V	J_{sc}/mA·cm^{-2}	FF/%	PCE[a] (Best[b])/%
PEDOT:PSS	0.61 ± 0.01	8.64 ± 0.38	55.92 ± 1.57	3.00 ± 0.18(3.18)
CuI	0.54 ± 0.01	8.69 ± 0.52	54.15 ± 2.23	2.55 ± 0.11(2.66)
C_3-SAM/CuI	0.55 ± 0.02	9.52 ± 0.43	56.43 ± 2.22	3.04 ± 0.16(3.20)

[a]The statistical results were obtained from 20 PSCs.

[b]Obtained from the best performance device.

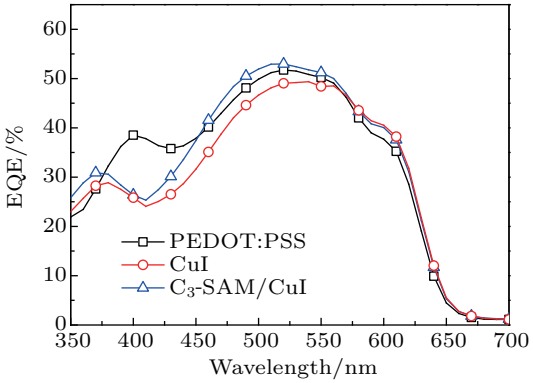


Fig. 7. (color online) EQE spectra of PSCs with PEDOT:PSS, CuI, and C_3-SAM/CuI as HTLs.

4. Conclusions

In conclusion, we have demonstrated a simple method of modifying the CuI HTLs with C_3-SAM on the surface of ITO to enhance the photovoltaic performance of PSCs. Due to the C_3-SAM incorporated between the ITO electrode and CuI layer, the CuI nanoparticles were much well-distributed on the surface of ITO and formed an uniform morphology with pinhole free and complete coverage. The best PCE of the devices based on C_3-SAM treatment reached 3.20%, which was similar to that of PSCs with PEDOT:PSS as HTLs. This work provides an effective strategy to control the morphology of CuI films and promotes the application of CuI as an attractive inorganic p-type material in efficient PSCs.

References

[1] Brabec C J, Gowrisanker S, Halls J J M, Laird D, Jia S J and Williams S P 2010 *Adv. Mater.* **22** 3839

[2] Kaltenbrunner M, White M S, Glowacki E D, Sekitani T, Someya T, Sariciftci N S and Bauer S 2012 *Nat. Commun.* **3** 1

[3] Li G, Zhu R and Yang Y 2012 *Nat. Photon.* **6** 153

[4] Zhang G G, Zhang K, Yin Q W, Jiang X F, Wang Z Y, Xin J M, Ma W, Yan H, Huang F and Cao Y 2017 *J. Am. Chem. Soc.* **139** 2387

[5] Wang J, Fei F, Luo Q, Nie S H, Wu N, Chen X L, Su W M, Li Y J and Ma C Q 2017 *Acs Appl. Mater. Inter.* **9** 7834

[6] Kim Y H, Spiegel D, Hotta S and Heeger A J 1988 *Phys. Rev. B* **38** 5490

[7] Liang Y Y, Xu Z, Xia J B, Tsai S T, Wu Y, Li G, Ray C and Yu L P 2010 *Adv. Mater.* **22** E135

[8] Zhang L J, He C, Chen J W, Yuan P, Huang L A, Zhang C, Cai W Z, Liu Z T and Cao Y 2010 *Macromolecules* **43** 9771

[9] Jia X P, Wu N, Wei J F, Zhang L P, Luo Q, Bao Z M, Li Y Q, Yang Y Z, Liu X G and Ma C Q 2016 *Org. Electron.* **38** 150

[10] Arias A C, Granström M, Thomas D S, Petritsch K and Friend R H 1999 *Phys. Rev. B* **60** 1854

[11] Smith C T G, Rhodes R W, Beliatis M J, Jayawardena K D G I, Rozanski L J, Mills C A and Silva S R P 2014 *Appl. Phys. Lett.* **105** 073304

[12] Wang T H, Chen C B, Guo K P, Chen G, Xu T and Wei B 2016 *Chin. Phys. B* **25** 038402

[13] Ahmadi M, Dafeh S R, Ghazanfarpour S and Khanzadeh M 2017 *Chin. Phys. B* **26** 097203

[14] Zhao W C, Li S S, Zhang S Q, Liu X Y and Hou J H 2017 *Adv. Mater.* **29** 1604059

[15] Li S S, Ye L, Zhao W C, Zhang S Q, Mukherjee S, Ade H and Hou J H 2016 *Adv. Mater.* **28** 9423

[16] Zhao F W, Dai S X, Wu Y, Zhang Q Q, Wang J Y, Jiang L, Ling Q D, Wei Z X, Ma W, You W, Wang C R and Zhan X W 2017 *Adv. Mater.* **29** 1700144

[17] Yan H, Lee P, Armstrong N R, Graham A, Evmenenko G A, Dutta P and Marks T J 2005 *J. Am. Chem. Soc.* **127** 3172

[18] Jørgensen M, Norrman K and Krebs F C 2008 *Sol. Energ. Mat. Sol. C* **92** 686

[19] Jin R, Levermore P A, Huang J S, Wang X H, Bradley D D C and Demello J C 2009 *Phys. Chem. Chem. Phys.* **11** 3455

[20] Hsu C C, Su H W, Hou C H, Shyue J J and Tsai F Y 2015 *Nanotechnology* **26** 385

[21] Rafique S, Abdullah S M, Mahmoud W E, Al-Ghamdi A A and Sulaiman K 2016 *Rsc Adv.* **6** 50043

[22] Zhang J, Wang J T, Fu Y Y, Zhang B H and Xie Z Y 2015 *Rsc Adv.* **5** 28786

[23] Chaudhary N, Chaudhary R, Kesari J P, Patra A and Chand S 2015 *J. Mater. Chem. C* **3** 11886

[24] Shao S Y, Liu J, Zhang J D, Zhang B H, Xie Z Y, Geng Y H and Wang L X 2012 *Acs Appl. Mater. Inter.* **4** 5704

[25] Sun W H, Peng H T, Li Y L, Yan W B, Liu Z W, Bian Z Q and Huang C H 2014 *J. Phys. Chem. C* **118** 16806

[26] Das S, Choi J Y and Alford T L 2015 *Sol. Energy Mat. Sol. Cells* **133** 255

[27] Mohamed S A, Gasiorowski J, Hingerl K, Zahn D R T, Scharber M C, Obayya S S A, El-Mansy M K, Sariciftci N S, Egbe D A M and Stadler P 2015 *Sol. Energy Mat. Sol. Cells* **143** 369

[28] Peng Y, Yaacobi-Gross X, Perumal A K, Faber H A, Vourlias G, Patsalas P A, D D C Bradley D C C, He Z and Anthopoulos T D 2015 *Appl. Phys. Lett.* **106** 243302

[29] Zhao K, Ndjawa G O N, Jagadamma L K, Labban A E, Hu H, Wang Q, Li R, Abdelsamie M, Beaujuge P M and Amassian A 2015 *Nano Energy* **16** 458

[30] Yoon S, Kim H, Shin E Y, Bae I G, Park B, Noh Y Y and Hwang I 2016 *Org. Electron.* **32** 200

[31] Yoon S, Kim H, Shin E Y, Noh Y Y, Park B and Hwang I 2016 *Phys. Status. Solidi. A* **213** 2431

[32] Patterson A L 1939 *Phys. Rev.* **56** 978

[33] Surajkumar Singh N, Dorendrajit Singh S, Dhiren Meetei S 2014 *Chin. Phys. B* **23** 058104

[34] Zuo L J, Gu Z W, Ye T, Fu W F, Wu G, Li H Y and Chen H Z 2015 *J. Am. Chem. Soc.* **137** 2674

[35] Gu Z W, Zuo L J, Larsen-Olsen T T, Ye T, Wu G, Krebs F C and Chen H Z 2015 *J. Mater. Chem. A* **3** 24254